Effects of momentum-dependent quasiparticle renormalization on the gap structure of iron-based superconductors

Shinibali Bhattacharyya,[1] P. J. Hirschfeld ⬥,[1] Thomas A. Maier ⬥,[2] and Douglas J. Scalapino[3]

[1]*Department of Physics, University of Florida, Gainesville, Florida 32611, USA*

[2]*Computational Sciences and Engineering Division and Center for Nanophase Materials Sciences,*
Oak Ridge National Laboratory, Oak Ridge, Tennessee 37831, USA

[3]*Department of Physics, University of California, Santa Barbara, California 93106, USA*

We discuss the influence of momentum-dependent correlations on the superconducting gap structure in iron-based superconductors. Within the weak coupling approach including self-energy effects at the one-loop spin-fluctuation level, we construct a dimensionless pairing strength functional which includes the effects of quasiparticle renormalization. The stationary solution of this equation determines the gap function at T_c. The resulting equations represent the simplest generalization of spin fluctuation pairing theory to include the effects of an anisotropic quasiparticle weight. We obtain good agreement with experimentally observed anisotropic gap structures in LiFeAs, indicating that the inclusion of quasiparticle renormalization effects in the existing weak-coupling theories can account for the observed anomalies in the gap structure of Fe-based superconductors.

I. INTRODUCTION

The role of electronic correlation effects on the properties of iron-based superconductors (FeSC) has been explored from a variety of different theoretical perspectives [1–6]. With the five d orbitals of Fe actively participating in low-energy processes, the possibility of orbital selective physics implies that weak correlations may exist in the states of electrons of one orbital type while strong correlations may occur in others. This may lead to substantial differences in quasiparticle weights, interactions, magnetism, and orbital ordering; in addition, Cooper pairing itself can become orbital selective [7–10]. This many-body mechanism augments the gap anisotropy that is already present in the conventional spin-fluctuation pairing model, proposed as the dominant source of Cooper pairing in FeSCs [11–13]. The usual argument leading to $s\pm$ pairing comes from interband pair scattering between electron and hole pockets facilitated by enhanced nesting [14]. Since the coherent d-orbital weight varies around any given Fermi surface sheet, gap anisotropy is present [15]. To the extent certain d orbitals are more incoherent than others due to correlations, pairing in these channels may be further suppressed, leading generally to enhanced gap anisotropy [16].

The degree of electronic correlation is known to vary considerably across the various families of Fe-based superconductors. Local-density approximation (LDA) + dynamical mean-field theory (DMFT) calculations have suggested that the 111 are considerably more correlated than, e.g., the well-studied 122 materials and that stronger interactions lead to a shrinkage of the inner hole pockets but the size and shape of the electron pockets [4,17,18] is maintained. Indeed, LiFeAs is one of several FeSCs known to have a Fermi surface which is quite different from what is predicted from den-

sity functional theory (DFT). Angle-resolved photoemission spectroscopy (ARPES) measurements [19,20] show that the Γ centered d_{xz}/d_{yz} hole pockets are considerably smaller than DFT predictions, and inclusion of local correlations within a DMFT scheme does not seem to solve this discrepancy. Recently, the Fermi surface was shown to be significantly renormalized via nonlocal correlations within a two-particle self-consistent approach [21], resembling ARPES findings.

Previous theoretical attempts [9,22–25] to understand the ARPES-determined gap structure [19,20,26,27] were based on a phenomenological tight-binding band structure consistent with ARPES data [23], i.e., describing the correct spectral positions of the bands. Despite some success in explaining some features of the gap structure, not all were reproduced properly; in particular, the large gaps on the inner hole pockets were not recovered in the conventional spin fluctuation treatments. Subsequently, Ref. [24] claimed a good overall fit to experiment by including vertex corrections.

In Ref. [16], a phenomenological approach assuming orbital selective renormalization of quasiparticle weights, primarily in the d_{xy} channel, was used to test the proposition that the discrepancies in calculated gap structures arose from self-energy effects neglected in conventional spin fluctuation theory. The results, applied to LiFeAs, FeSe crystals, and FeSe monolayers showed good agreement with measured magnitudes and anisotropies of gaps from ARPES [20] and Bogoliubov quasiparticle interference (BQPI) experiments [26], and yielded quasiparticle weights qualitatively consistent with LDA+DMFT and other normal state studies. While this approach lacked a microscopic framework within which to calculate the quasiparticle weights, it showed that quasiparticle renormalization effects were important.

These effects have previously been treated within the fluctuation exchange approximation (FLEX) [28–30] but here

we explore a multiorbital random-phase approximation (RPA) which is more simply related to the results of the phenomenological treatment [16]. The approach we discuss in here can be considered as a Fermi surface restricted one-loop FLEX calculation. As such, it does not involve any ad-hoc restrictions and is numerically much less expensive. In our approach, the spin and charge fluctuations are treated within the RPA and their effect on both the paring and the single particle self-energy channels are approximated by the zero frequency RPA interactions on the Fermi surface.

In Sec. II we introduce the five-orbital tight-binding model that we will study along with the multiorbital RPA effective interactions. Following this, the eigenvalue equation for the pairfield strength and the gap function along with the equation for the single particle renormalization factor are discussed. In Sec. III we demonstrate the results of solving these equations for LiFeAs, and discuss this in comparison to experiments (Sec. III A). In Sec. III B we analyze our results in terms of the quasiparticle renormalization weights and the pairing vertex, and in the following Sec. III C we discuss the tendency of iron-based systems towards $s^\pm$ pairing symmetry due to electronic correlations. Finally, we note the improvement obtained in predicting the pairing structure when the single particle self-energy is included. In the Appendix we give the derivation of the dimensionless pairing strength functional and the resulting stationary eigenvalue equation for the pairing strength and gap function.

II. MODEL

We start with a five-orbital tight-binding Hamiltonian H_0 and include local interactions via Hubbard-Hund terms:

$$
\begin{aligned}
H &= H_0 + H_I \\
&= \sum_{ij\sigma} \sum_{qt} \left(t_{ij}^{tq} - \mu_0 \delta_{ij} \delta_{tq} \right) c_{it\sigma}^\dagger c_{jq\sigma} \\
&\quad + U \sum_{it} n_{it\uparrow} n_{it\downarrow} + U' \sum_{i,t<q} \sum_{\sigma\sigma'} n_{it\sigma} n_{iq\sigma'} \\
&\quad + J \sum_{i,t<q} \sum_{\sigma\sigma'} c_{it\sigma}^\dagger c_{iq\sigma'}^\dagger c_{it\sigma'} c_{iq\sigma} \\
&\quad + J' \sum_{i,t\neq q} c_{it\uparrow}^\dagger c_{iq\downarrow}^\dagger c_{it\downarrow} c_{iq\uparrow},
\end{aligned}
\tag{1}
$$

where the interaction parameters U, U', J, J' are given in the notation of Kuroki *et al.* [31]. We consider cases which obey spin-rotation invariance (SRI) through the relations $U' = U - 2J$ and $J = J'$. The kinetic energy H_0 includes the chemical potential μ_0 and is described by a tight-binding model spanned by five Fe d orbitals $[d_{xy}, d_{x^2-y^2}, d_{xz}, d_{yz}, d_{3z^2-r^2}]$. Here q and t are the orbital indices and i, j is the Fe-atom site. The spectral representation of the noninteracting Green's function is

$$
G_{tq}^0(\mathbf{k}, \omega_m) = \sum_\mu \frac{a_\mu^t(\mathbf{k}) a_\mu^{q*}(\mathbf{k})}{i\omega_m - E_\mu(\mathbf{k})},
\tag{2}
$$

where the matrix elements $a_\mu^q(\mathbf{k}) = \langle q | \mu \mathbf{k} \rangle$ are spectral weights of the Bloch state $|\mu\mathbf{k}\rangle$ with band index μ and wave vector $\mathbf{k}$ in the orbital basis and $\omega_m = (2m + 1)\pi k_B T$ are the

fermionic Matsubara frequencies for a given temperature T. We will adopt Latin symbols to denote orbital indices and Greek ones to denote band indices, throughout the rest of the discussion.

The orbitally resolved noninteracting susceptibility is

$$
\begin{aligned}
\chi_{pqst}^0(\mathbf{q}, \Omega_m) &= -\frac{1}{N_k \beta} \sum_{\mathbf{k}\omega_m} G_{tq}^0(\mathbf{k}, \omega_m) G_{ps}^0(\mathbf{k}+\mathbf{q}, \omega_m + \Omega_m) \\
&= -\frac{1}{N_k} \sum_{\mathbf{k}\mu\nu} \frac{a_\mu^t(\mathbf{k}) a_\mu^{q*}(\mathbf{k}) a_\nu^p(\mathbf{k}+\mathbf{q}) a_\nu^{s*}(\mathbf{k}+\mathbf{q})}{i\Omega_m + E_\mu(\mathbf{k}) - E_\nu(\mathbf{k}+\mathbf{q})} \\
&\quad \times \{ f(E_\mu[\mathbf{k}]) - f[E_\nu(\mathbf{k}+\mathbf{q})] \},
\end{aligned}
\tag{3}
$$

where N_k is the number of Fe lattice sites, $\beta = 1/k_B T$ is the inverse temperature, and $\Omega_m = 2m\pi k_B T$ is the bosonic Matsubara frequency. Within the RPA, the charge-fluctuation and spin-fluctuation parts of the RPA susceptibility are given by

$$
\begin{aligned}
\chi^C(\mathbf{q}, \Omega_m) &= [1 + \chi^0(\mathbf{q}, \Omega_m) U^C]^{-1} \chi^0(\mathbf{q}, \Omega_m), \\
\chi^S(\mathbf{q}, \Omega_m) &= [1 - \chi^0(\mathbf{q}, \Omega_m) U^S]^{-1} \chi^0(\mathbf{q}, \Omega_m).
\end{aligned}
\tag{4}
$$

The interaction matrices U^C and U^S in orbital space have the following elements:

$$
\begin{array}{ll}
U_{pppp}^C = U, & U_{pppp}^S = U, \\
U_{ppss}^C = 2U' - J, & U_{ppss}^S = J, \\
U_{pssp}^C = J', & U_{pssp}^S = J', \\
U_{psps}^C = 2J - U', & U_{psps}^S = U'.
\end{array}
\tag{5}
$$

Defining $U^{SC} = U^S + U^C$, the particle-hole (N) and the singlet pairing particle-particle (A) interactions are

$$
\begin{aligned}
[V_{pqst}(\mathbf{q}, \Omega_m)]_N &= \left[\frac{3}{2} U^S \chi^S(\mathbf{q}, \Omega_m) U^S + \frac{3U^S}{2} \right. \\
&\quad + \frac{1}{2} U^C \chi^C(\mathbf{q}, \Omega_m) U^C - \frac{U^C}{2} \\
&\quad \left. - \frac{1}{4} U^{SC} \chi^0(\mathbf{q}, \Omega_m) U^{SC} \right]_{pqst}, \\
[V_{pqst}(\mathbf{q}, \Omega_m)]_A &= \left[\frac{3}{2} U^S \chi^S(\mathbf{q}, \Omega_m) U^S + \frac{U^S}{2} \right. \\
&\quad \left. - \frac{1}{2} U^C \chi^C(\mathbf{q}, \Omega_m) U^C + \frac{U^C}{2} \right]_{pqst}.
\end{aligned}
\tag{6}
$$

In the following we assume that the dynamics of the interaction is cut off on a spin-fluctuation energy scale and we will restrict the treatment of the problem to Bloch states on the Fermi surface. We have assumed that the leading pairing instability occurs in the even-frequency channel. Odd-frequency pairing, if it occurs, is expected to be associated with a reduced critical temperature [32]. Assuming that no bands cross each other in the vicinity of the Fermi level (i.e., $\Omega_m = \Omega = 0$ eV), each Fermi momentum point corresponds to a unique band quantum number, i.e., $\mathbf{k} \in \mu$ and $\mathbf{k}' \in \nu$. The corresponding band representation for the interaction vertices, describing scattering of particles between $(\mathbf{k}_\mu, \mathbf{k}_\nu')$ states at the
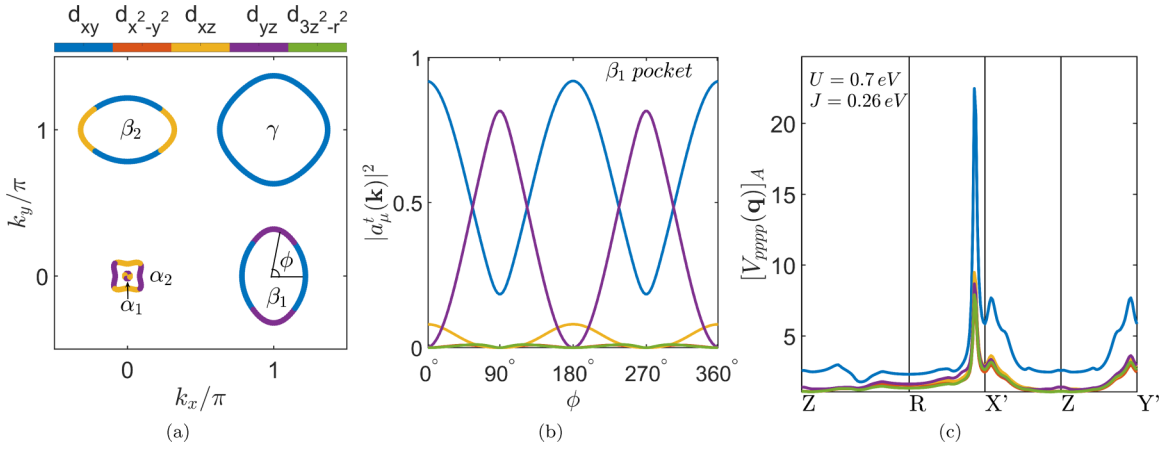
FIG. 1. (a) Fermi surface at $k_z = \pi$ plane for LiFeAs represented by its corresponding dominant orbital character as indicated in the color legend. (b) Orbital weight along the β_1 electron pocket plotted as a function of angle ϕ shown in (a). (c) Diagonal orbital components of the static particle-particle effective interaction $[V_{pppp}(\mathbf{q}, 0)]_A$ along high-symmetry path Z-R-X'-Z-Y' with U and J as indicated. Plots as a function of the angle ϕ around the Fermi pockets are done with the angle measured counterclockwise from the k_x axis.

Fermi level, is

$$[V(\mathbf{k}_\mu, \mathbf{k}'_\nu, 0)]_N = \mathrm{Re} \sum_{pqst} \left\{ a_\mu^{q*}(\mathbf{k}_\mu) a_\nu^{s*}(\mathbf{k}'_\nu) \right.$$
$$\left. \times [V_{pqst}(\mathbf{k}_\mu - \mathbf{k}'_\nu, 0)]_N a_\mu^t(\mathbf{k}_\mu) a_\nu^p(\mathbf{k}'_\nu) \right\},$$

$$[V(\mathbf{k}_\mu, \mathbf{k}'_\nu, 0)]_A = \mathrm{Re} \sum_{pqst} \left\{ a_\mu^{p*}(\mathbf{k}_\mu) a_\mu^{t*}(-\mathbf{k}_\mu) \right.$$
$$\left. \times \left[V_{pqst}(\mathbf{k}_\mu - \mathbf{k}'_\nu, 0) \right]_A a_\nu^q(\mathbf{k}'_\nu) a_\nu^s(-\mathbf{k}'_\nu) \right\}.$$
$$(7)$$

The symmetrized singlet pairing vertex is then given by

$$[V(\mathbf{k}_\mu, \mathbf{k}'_\nu, 0)]_A = \tfrac{1}{2} \{ [V(\mathbf{k}_\mu, \mathbf{k}'_\nu, 0)]_A + [V(-\mathbf{k}_\mu, \mathbf{k}'_\nu, 0)]_A \}.$$
$$(8)$$

As discussed in the Appendix A, the stationary solution of the pairing strength functional [Eq. (A22)] is determined by the eigenvalue equation:

$$\lambda g(\mathbf{k}_\mu) = -\frac{1}{(2\pi)^d} \oint_{\mathbf{k}'_\nu \in FS} \frac{[V(\mathbf{k}_\mu, \mathbf{k}'_\nu, 0)]_A}{Z(\mathbf{k}'_\nu)} \frac{d^{d-1}k'_\nu}{|\mathbf{v}_F(\mathbf{k}'_\nu)|} g(\mathbf{k}'_\nu),$$
$$(9)$$

with

$$Z(\mathbf{k}_\mu) = 1 + \frac{1}{(2\pi)^d} \oint_{\mathbf{k}'_\nu \in FS} [V(\mathbf{k}_\mu, \mathbf{k}'_\nu, 0)]_N \frac{d^{d-1}k'_\nu}{|\mathbf{v}_F(\mathbf{k}'_\nu)|}. \quad (10)$$

Here $\mathbf{v}_F(\mathbf{k}'_\nu)$ is the Fermi velocity of band ν and the integration is over its corresponding Fermi surface. The eigenfunction $g(\mathbf{k}_\mu)$ then determines the symmetry and structure of the leading pairing gap close to T_c. Traditional spin-fluctuation pairing calculation sets $Z(\mathbf{k}_\mu)$ to unity. Instead, we use the solution for $Z(\mathbf{k}_\mu)$ from Eq. (10) in Eq. (9). Solving Eq. (9) for the eigenfunction $g(\mathbf{k}_\mu)$ corresponding to the leading eigenvalue λ gives the modified gap function $\Delta(\mathbf{k}_\mu) = \frac{g(\mathbf{k}_\mu)}{Z(\mathbf{k}_\mu)}$. Note that we adopt here the notation $Z(\mathbf{k})$ consistent with Eliashberg's convention, such that $Z \gg 1$ corresponds to a highly incoherent quasiparticle. This is in contrast to the notation adopted in much of the orbital selective literature,

where Z rather than Z^{-1} is the quasiparticle weight (see, e.g., Sprau *et al.* [10]).

In the results presented here, we perform 2D calculations with a $\mathbf{k}$ mesh on the order of 100×100 in the unfolded Brillouin zone (BZ), and ≈ 500 total number of Fermi surface points. We set $k_B T = 0.01$ eV for the rest of this paper.

III. RESULTS

To study the effects of momentum-dependent correlations on the pairing structure, we have chosen the electronic dispersion relevant to LiFeAs as in Ref. [23]. Certain Fermi sheets in LiFeAs are known to have significant k_z dispersion. However, to compare with experimental data of measured gap magnitudes, we only consider the $k_z = \pi$ plane for our analysis, where all the $Z = (0, 0, \pi)$-centered hole pockets are present. We stress that the 3D properties of the dispersion do not affect the conclusions of our results, since $\chi(\mathbf{q}, 0)$ is nearly independent of q_z [23].

As shown in Fig. 1(a), for the undoped material with a filling of $n = 6$ in the 1-Fe BZ, the Fermi surfaces include two small hole pockets α_1 and α_2 at the Z point with dominant d_{xz}/d_{yz} orbital characters, a large hole pocket γ at the $R = (\pi, \pi, \pi)$ point of predominantly d_{xy} orbital character, and two electron pockets β_1 (β_2) situated at $X' = (\pi, 0, \pi)$ [$Y' = (0, \pi, \pi)$] points of d_{yz}/d_{xy} (d_{xz}/d_{xy}) orbital characters. Since the Y'-centered pocket is symmetry related to the X' pocket in this tetragonal system, it will not be discussed separately. In Fig. 1(b) we show the corresponding orbital weight $|a_\mu^t(\mathbf{k})|^2$ for the β_1 pocket as a function of the angle ϕ. We will relate this to $Z(\mathbf{k}_\mu)$ and the modulation in gap amplitude in the following analysis of our results.

Now we will present our solutions to Eqs. (9) and (10) for $Z(\mathbf{k}_\mu)$ and the leading pairing eigenvectors (gap functions). We have evaluated the results for two sets of Hubbard-Hund parameters ($U = 0.7$ eV, $J = 0.26$ eV) and ($U = 0.79$ eV, $J = 0.2$ eV). These parameters are close to the standard parameters used in the literature employing the RPA approach to the pairing vertex.
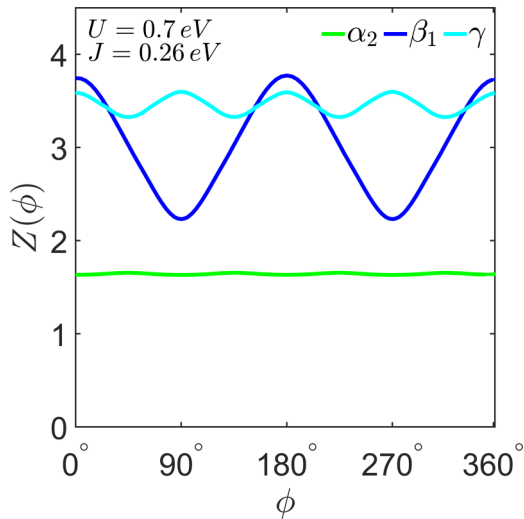
FIG. 2. $Z(\phi)$ along Fermi pockets α_2, β_1, and γ evaluated from the static particle-hole effective interaction defined in Eq. (10).

First, we will discuss the results for $U = 0.7$ eV, $J = 0.26$ eV and compare with experimental data. In Fig. 1(c) the diagonal components of the static particle-particle effective interaction $[V_{pppp}(\mathbf{q}, 0)]_A$ evaluated from Eq. (6) is plotted along the high-symmetry path Z-R-X'-Z-Y'. The RPA susceptibility shows an enhanced incommensurate peak around $\mathbf{q} = \pi(1, 0.15)$ (similar to the findings in Ref. [23]). The d_{xy} orbital channel is the largest in magnitude as a consequence of favorable nesting condition between d_{xy}-dominated parts of the electron pocket at X'/Y' and the hole pocket at R. The phase space for scattering of quasiparticles between the d_{xz}/d_{yz}-dominated parts of the Fermi surfaces is restricted due to small pocket sizes of the α hole pockets and their unfavorable nesting conditions in connection to the electron pockets. Thus, the magnitude of the d_{xz}/d_{yz} orbital channel for $[V_{pppp}(\mathbf{q}, 0)]_A$ is much lower than the d_{xy} channel. Both the static particle-particle effective interaction $[V_{pqst}(\mathbf{q}, 0)]_A$ and particle-hole effective interaction $[V_{pqst}(\mathbf{q}, 0)]_N$ is dominated

by the RPA spin-susceptibility contribution, and hence their underlying momentum structure is similar.

In Fig. 2 we plot $Z(\mathbf{k}_\mu)$ evaluated from Eq. (10) as a function of the angle ϕ around the α_2, β_1, and γ Fermi pockets. Evidently, $Z(\phi)$ around the β_1 pocket follows the orbital content of the d_{xy} orbital [compare to Fig. 1(b) for an angular plot of the orbital weight around the β_1 pocket]. This is expected from the current Fermi surface topology depending on two factors: (1) the interaction vertices are dominated by intraorbital processes, and (2) the d_{xy} orbital with large weight at certain positions on the Fermi surface can take advantage of the strong peak in the susceptibility for scattering vectors $\mathbf{k}_\mu - \mathbf{k}'_\nu \approx \pi(1, 0.15)$ roughly connecting $\mathbf{k}_\mu$ and $\mathbf{k}'_\nu$ across Fermi pockets. For the β_1 pocket, this happens around $[0°, 180°]$. For the γ pocket, maxima in $Z(\phi)$ are seen at $[0°, 90°, 180°, 270°]$. Due to the lower magnitude of the $[V_{pppp}(\mathbf{q}, 0)]_N$ vertex for the d_{xz}/d_{yz} orbitals, the magnitude of $Z(\phi)$ around the α_2 pocket is smaller than around the β_1 and γ pockets.

A. Gap structure

We show the results for the leading gap structure in Fig. 3(a) obtained from traditional spin-fluctuation calculation with $Z(\mathbf{k}'_\nu)$ set to unity in Eq. (9). Figure 3(b) is the most important result of this work, displaying the modified gap structure obtained by inclusion of momentum-dependent correlation effects $Z(\mathbf{k}_\mu) \neq 1$ via the linearized Eliashberg equations (9) and (10). For comparison of our calculations to experimental results, we have plotted C_4-symmetrized ARPES data for the gap magnitude taken from Ref. [20] and BQPI data from Ref. [26] for the three Fermi pockets α_2, β_1, γ in Fig. 3(c). ARPES sees only one band crossing at the Fermi level at Z on the $k_z = \pi$ plane with a large gap of the order of 6 meV. However, our current DFT-derived tight-binding structure always produces two α pockets. Hence, we will consider it to be roughly appropriate to speak of an average gap on the α pockets assigned to α_2. In both Figs. 3(a) and 3(b) we find an $s^\pm$-wave state with highly anisotropic but full

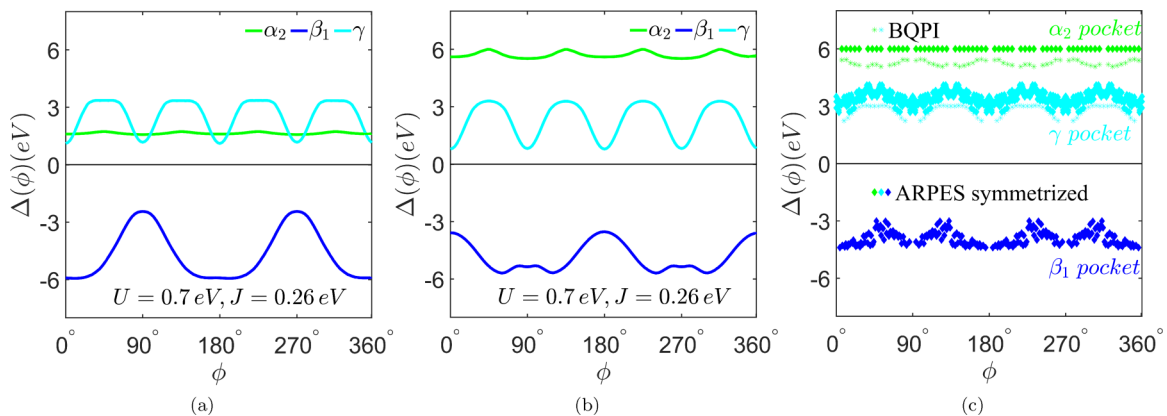(a)   (b)   (c)

FIG. 3. Results for LiFeAs: (a) Angular plot of the s-wave gap function evaluated from traditional spin-fluctuation theory, around the Z-centered outer hole pocket α_2, X'-centered electron pocket β_1, and R-centered hole pocket γ. (b) The modified gap function obtained from the linearized Eliashberg equations (9) and (10) with quasiparticle renormalization $Z(\mathbf{k})$ included. (c) Experimental results: Measured magnitudes of the gap from an ARPES experiment [20], symmetrized and displayed as diamonds and those from Bogoliubov QPI experiment [26] displayed as crosses. All calculations are done for U and J as indicated.
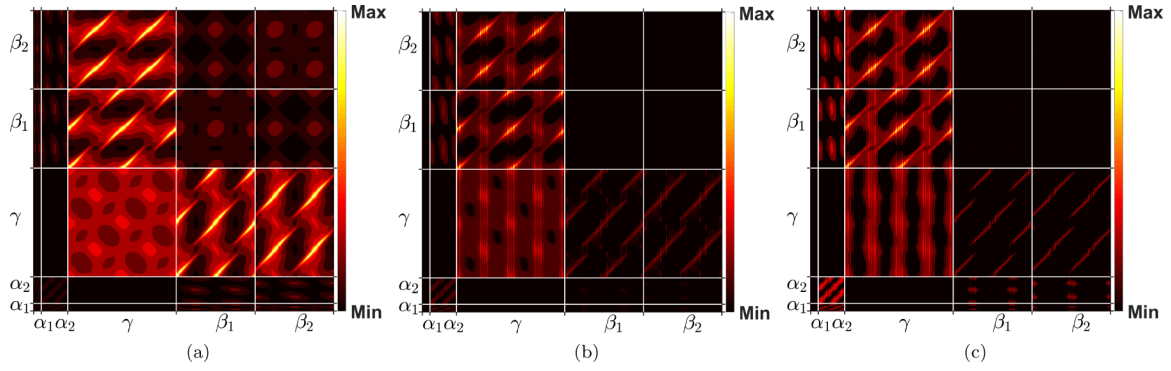
FIG. 4. Heat map plots of (a) the singlet pairing vertex $[V(\mathbf{k}_\mu, \mathbf{k}'_\nu, 0)]_A$ matrix resulting in the gap function plotted in Fig. 3(a) from the tight-binding model. (b) Matrix elements of the quantity $[V(\mathbf{k}_\mu, \mathbf{k}'_\nu, 0)]_A dk'_\nu / |\mathbf{v}_F(\mathbf{k}'_\nu)|$. (c) Matrix elements of the quantity $[V(\mathbf{k}_\mu, \mathbf{k}'_\nu, 0)]_A dk'_\nu / |\mathbf{v}_F(\mathbf{k}'_\nu)| / Z(\mathbf{k}'_\nu)$. The value at any given point is proportional to the brightness of the color. The rows and the columns of the tiles of (a)–(c) correspond to the Fermi points $\mathbf{k}_\mu$ and $\mathbf{k}'_\nu$ arranged in ascending order of their corresponding polar angle $\phi = 0°$ to $360°$ around each Fermi sheet. Band indices μ and ν represent the Fermi sheets α_1, α_2 at the Z, γ at the R, β_1 at the X', and β_2 at the Y' point. Unequal areas of the tiles are due to unequal number of Fermi points around each of the sheets.

gaps on the electron (negative gap) and hole (positive gap) pockets.

With self-energy effects included, the gap functions undergo a remarkable change [Fig. 3(b)] relative to the traditional spin-fluctuation calculation [Fig. 3(a)]. First, we find a stronger tendency towards $s^\pm$ pairing symmetry, even for small values of J. We will discuss this in further detail in Sec. III C. Second, $Z(\mathbf{k}_\mu)$ induces a momentum-dependent modulation of the gap function on various pockets. Most importantly, in Fig. 3(b) we see that $Z(\mathbf{k}_\mu)$ enhances the magnitude of the nearly isotropic gap on the small Z-centered hole pocket α_2. This brings the results of spin-fluctuation theory much closer in line with experimental data, and corrects the crucial discrepancy in the calculation of Wang *et al.* [23] relative to experiment. Although the angular positions of the gap maxima and minima on the γ pocket and the average gap magnitude is in agreement with experiment, we do not obtain a suppression of the anisotropy. We find weaker anisotropy of the gap function on the β_1 pocket and an average gap magnitude comparable to experiment. However, the theoretical gap structure has two global maxima as opposed to four in the experimental data, and these maxima are located at positions where the experimental data has minima. In the next section we will analyze the results for the gap structure in terms of the quasiparticle renormalization factor $Z(\mathbf{k}_\mu)$ and the pairing vertex.

B. Analysis of the gap structure in terms of quasiparticle weights and the pairing vertex

We investigate the structure of the effective pair vertex from its graphical representation in Figs. 4(a)–4(c). Each block demarcated by white lines in the image represents a matrix $(\mathbf{k}_\mu, \mathbf{k}'_\nu)$ consisting of values corresponding to the pairing vertex, with the Fermi points $\mathbf{k}_\mu$ and $\mathbf{k}'_\nu$ arranged in ascending order of their corresponding polar angle $\phi = 0°$ to $360°$ around each Fermi sheet $(\alpha_1, \alpha_2, \beta_1, \beta_2, \gamma)$. By construction, as in Eq. (8), $[V(\mathbf{k}_\mu, \mathbf{k}'_\nu, 0)]_A$ is a symmetric matrix with respect to the interchange $\mathbf{k}_\mu \leftrightarrow \mathbf{k}'_\nu$ as seen in Fig. 4(a). Figure 4(b) shows matrix elements of the quantity

$[V(\mathbf{k}_\mu, \mathbf{k}'_\nu, 0)]_A dk'_\nu / |\mathbf{v}_F(\mathbf{k}'_\nu)|$. This is the matrix which is diagonalized in traditional spin-fluctuation theory to obtain the leading eigenstate. It is not symmetric under the exchange $\mathbf{k}_\mu \leftrightarrow \mathbf{k}'_\nu$. Here dk'_ν is the length element of the Fermi sheet at the k'_νth Fermi point. The factor $1/|\mathbf{v}_F(\mathbf{k}'_\nu)|$ acts as a momentum-dependent density of states for the corresponding band ν at the Fermi level.

In the figures the brightest set of blocks are the ones representing scattering processes among the pockets γ and β_1 (β_2). It is visually prominent that the dominant scattering processes occur for $\gamma \rightarrow \beta_1$ (β_2). As discussed earlier, scattering between the d_{xy}-dominated part of the Fermi pockets contributes to the primary pairing interaction leading to superconductivity. Although angular positions of $[0°, 90°, 180°, 270°]$ on the γ pocket are favored to take advantage of the d_{xy}-dominated scattering to either β_1 or β_2 pocket, positions of $[45°, 135°, 225°, 315°]$ take advantage of simultaneous scattering to β_1 and β_2 pockets. This renders gap maxima around $[45°, 135°, 225°, 315°]$ on the γ pocket [refer to Fig. 3(a)]. It also explains why gap maxima occur at $[0°, 180°]$ on the β_1 pocket due to favorable d_{xy} scattering to the γ pocket. Due to restricted scattering between α_2 and the other pockets, the overall gap magnitude is very low on this pocket.

In Fig. 4(c) we show matrix elements of the quantity $[V(\mathbf{k}_\mu, \mathbf{k}'_\nu, 0)]_A dk'_\nu / |\mathbf{v}_F(\mathbf{k}'_\nu)| / Z(\mathbf{k}'_\nu)$. The leading eigenfunction $g(\mathbf{k}_\mu)$ of this matrix gives the modified gap function as $\Delta(\mathbf{k}_\mu) = \frac{g(\mathbf{k}_\mu)}{Z(\mathbf{k}_\mu)}$. Compared to Fig. 4(b), the first noticeable difference is the enhanced pairing (brighter spots) occurring between the α_2 pocket and the β_1 (β_2) pockets. It appears as if the electronic correlations tend to lift the restriction on the phase space of scattering between the non-nested d_{xz}/d_{yz}-dominated parts of the α_2 Fermi pocket. This is one of the main effects of the momentum-dependent modulation of the pairing vertex due to $Z(\mathbf{k}'_\nu)$. In addition, due to the smaller magnitude of $Z(\mathbf{k}_{\alpha_2})$ (refer to Fig. 2), the final gap function $\Delta(\mathbf{k}_{\alpha_2})$ undergoes further enhancement in its magnitude as seen in Fig. 3(b). We also find that the gap maxima shifts to $[90°, 270°]$ on the β_1 pocket due to enhanced pairing to the α_2 pocket via the d_{yz} orbitals, combined with the effect of
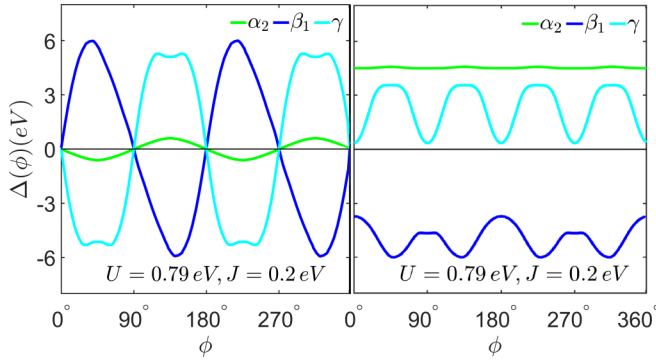
FIG. 5. Angular plots of the gap function evaluated around the Fermi pockets as indicated by the color legend. The calculations show a change in the gap symmetry of the leading eigenfunction from (left) d wave (obtained from traditional spin-fluctuation theory with $Z(\mathbf{k}) = 1$) to (right) s wave [obtained from linearized Eliashberg equations with $Z(\mathbf{k})$ included]. Both calculations are done for U and J as indicated.

momentum modulation by $Z(\mathbf{k}_{\beta_1})$ on the final gap function. The γ and β_1 (β_2) pocket pairing is not affected substantially due to the $Z(\mathbf{k}'_\nu)$ modulation. Hence, $\Delta(\mathbf{k}_\gamma)$ does not undergo any drastic changes.

C. Discussion: Tendency towards $s\pm$ pairing symmetry

A close competitor of the leading $s\pm$ state is the d-wave state, which has never been convincingly observed in any experiment in the context of FeSCs. In the traditional spin-fluctuation scenario, d and s wave solutions are nearly degenerate in LiFeAs [23], a consequence of its poor $(\pi, 0)$ nesting properties [17,19,33]. In Fig. 5 we show the results for calculations with Hubbard-Hund parameters ($U = 0.79$ eV, $J = 0.2$ eV) [which is a higher U and a lower J value than the previous calculation shown in Figs. 3(a) and 3(b)]. With this particular set of U and J, the traditional spin-fluctuation theory yields a d-wave state as the leading pairing state (left panel in Fig. 5). We see a sign change in the gap structure around each pocket ($\alpha_2, \beta_1, \gamma$) with a periodicity of $\pi/2$. For this case, the second leading eigenchannel is the s-wave channel and the ratio of their eigenvalues is $\lambda_d/\lambda_s = 1.05$. In contrast, the inclusion of correlations effect via the linearized Eliashberg equations (9) and (10) stabilizes the s-wave state as the leading eigenfunction, and the d-wave state becomes subleading. For this case we get $\lambda_d/\lambda_s = 0.97$. This points towards quasiparticle renormalization effects playing an important role in stabilizing the $s\pm$ pairing state in LiFeAs.

IV. CONCLUSIONS

We have performed 2D calculations of the superconducting pairing state for the LiFeAs compound, one of the few materials where ARPES experiments have measured the gap function on several different Fermi surface sheets, and found significant gap anisotropy. As a test of the proposal that a proper treatment of momentum dependent quasiparticle renormalization is the major missing ingredient in traditional spin fluctuation calculations of gap structures in FeSC, we have provided a simple approximate theoretical framework for the

calculation of the superconducting gap from spin fluctuation theory, including momentum-dependent self-energy effects at the single-particle level. We have shown that this approach leads to robust $s\pm$ pairing of the conventional type, and provides substantial improvement of the calculated gap structure on all the Fermi pockets compared to experiments, especially for the large gap on the inner hole pocket. We have calculated the leading stationary solution of a spin-fluctuation pairing strength functional which includes quasiparticle self-energy effects, and discussed their role in stabilizing the $s\pm$ eigenstate. We conclude that the inclusion of self-energy effects within the framework of existing weak-coupling theories is an important ingredient to understand the observed superconducting pairing structures in LiFeAs, and other FeSCs, which are dictated by the same underlying physical processes. Vertex corrections as calculated in Ref. [24] do not appear to be necessary to capture the basic renormalization of the electronic structure and pairing vertex.

APPENDIX: A SPIN-FLUCTUATION PAIRING STRENGTH FUNCTIONAL INCLUDING QUASIPARTICLE RENORMALIZATION

In the multiband Nambu basis given by

$$\Psi_{\alpha\mathbf{k}} = \begin{pmatrix} c_{\alpha,\mathbf{k}\uparrow} \\ c_{\alpha,-\mathbf{k}\downarrow}^\dagger \end{pmatrix}, \quad \Psi_{\alpha\mathbf{k}}^\dagger = (c_{\alpha,\mathbf{k}\uparrow}^\dagger, \, c_{\alpha,-\mathbf{k}\downarrow})$$

the band index α ranges from 1 to 5 in FeSCs equal to the number of Fe $3d$ orbitals. We express the noninteracting Hamiltonian as $H_0 = \sum_{\alpha\mathbf{k}} \varepsilon_\alpha(\mathbf{k})\Psi_{\alpha\mathbf{k}}^\dagger \tau_3 \Psi_{\alpha\mathbf{k}}$ where $\varepsilon_\alpha(\mathbf{k})$ is the dispersion in the α band in the normal state of the system. The Pauli matrices are denoted conventionally by τ_i, $i = 0, 1, 2, 3$. The Hamiltonian H_0, the full renormalized Green's function $\underline{G}(\mathbf{k}, \omega_m)$, the noninteracting Green's function $\underline{G}_0(\mathbf{k}, \omega_m)$, and the self-energy $\underline{\Sigma}(\mathbf{k}, \omega_m)$ are all 10×10 matrices in this multiband basis for every set of $(\mathbf{k}, \omega_m)$. The noninteracting band Green's function $G_{\alpha 0}(\mathbf{k}, \omega_m) = [i\omega_m - \varepsilon_\alpha(\mathbf{k})]^{-1}$ gives the full matrix as $\underline{G}_0(\mathbf{k}, \omega_m) = [i\omega_m\tau_0 - \varepsilon_\alpha(\mathbf{k})\tau_3]^{-1}$. The particle-hole and the particle-particle Green's function

are defined, respectively, as

$$G_\alpha(\mathbf{k}, \omega_m) = -\int_0^\beta d\tau e^{i\omega_m\tau} \langle T_\tau c_{\alpha,\mathbf{k}\sigma}(\tau) c^\dagger_{\alpha,\mathbf{k}\sigma}(0)\rangle,$$

$$F_\alpha(\mathbf{k}, \omega_m) = \int_0^\beta d\tau e^{i\omega_m\tau} \langle T_\tau c_{\alpha,\mathbf{k}\uparrow}(\tau) c_{\alpha,-\mathbf{k}\downarrow}(0)\rangle,$$

(A1)

and the corresponding full Green's function:

$$\underline{G}(\mathbf{k}, \omega_m) = \begin{pmatrix} G_\alpha(\mathbf{k}, \omega_m) & F_\alpha(\mathbf{k}, \omega_m) \\ F^*_\alpha(\mathbf{k}, \omega_m) & -G_\alpha(-\mathbf{k}, -\omega_m) \end{pmatrix}.$$

The full self-energy is

$$\underline{\Sigma}(\mathbf{k}, \omega_m) = \begin{pmatrix} \Sigma_\alpha(\mathbf{k}, \omega_m) & \Phi_\alpha(\mathbf{k}, \omega_m) \\ \Phi^*_\alpha(\mathbf{k}, \omega_m) & -\Sigma_\alpha(-\mathbf{k}, -\omega_m) \end{pmatrix}, \quad (A2)$$

where the particle-hole and particle-particle components are given by

$$\Sigma_\alpha(\mathbf{k}, \omega_m) = \frac{1}{\beta N_{k'}} \sum_{n,\beta,\mathbf{k}'} V_{\alpha\beta N}(\mathbf{k} - \mathbf{k}', \omega_m - \omega_n) G_\beta(\mathbf{k}', \omega_n),$$

$$\Phi_\alpha(\mathbf{k}, \omega_m) = \frac{1}{\beta N_{k'}} \sum_{n,\beta,\mathbf{k}'} V_{\alpha\beta A}(\mathbf{k} - \mathbf{k}', \omega_m - \omega_n) F_\beta(\mathbf{k}', \omega_n).$$

(A3)

The particle-hole interaction between band α and β is denoted by $V_{\alpha\beta N}(\mathbf{k} - \mathbf{k}', \omega_m - \omega_n)$, whereas the particle-particle interaction is denoted by $V_{\alpha\beta A}(\mathbf{k} - \mathbf{k}', \omega_m - \omega_n)$. From Dyson's equation we have

$$\underline{G}^{-1}(\mathbf{k}, \omega_m) = \underline{G}_0^{-1}(\mathbf{k}, \omega_m) - \underline{\Sigma}(\mathbf{k}, \omega_m). \quad (A4)$$

Using the Pauli matrices, $\underline{\Sigma}$ can be written as

$$\underline{\Sigma}(\mathbf{k}, \omega_m) = i\omega_m[1 - Z_\alpha(\mathbf{k})]\tau_0 + X_\alpha(\mathbf{k}, \omega_m)\tau_3$$
$$+ \Phi_\alpha(\mathbf{k}, \omega_m)\tau_1 + \overline{\Phi_\alpha}(\mathbf{k}, \omega_m)\tau_2, \quad (A5)$$

with yet unknown and independent functions $Z_\alpha(\mathbf{k})$, $X_\alpha(\mathbf{k}, \omega_m)$, $\Phi_\alpha(\mathbf{k}, \omega_m)$, $\overline{\Phi_\alpha}(\mathbf{k}, \omega_m)$. From Dyson's Eq. (A4) and the Pauli matrix identity $(a_0\tau_0 + \vec{a}.\vec{\tau})(a_0\tau_0 - \vec{a}.\vec{\tau}) = (a_0^2 - \vec{a}^2)\tau_0$, one finds

$$\underline{G}(\mathbf{k}, \omega_m) = \{i\omega_m Z_\alpha(\mathbf{k})\tau_0 + [\varepsilon_\alpha(\mathbf{k}) + X_\alpha(\mathbf{k}, \omega_m)]\tau_3$$
$$+ \Phi_\alpha(\mathbf{k}, \omega_m)\tau_1 + \overline{\Phi_\alpha}(\mathbf{k}, \omega_m)\tau_2\}/D_\alpha(\mathbf{k}, \omega_m),$$

(A6)

with $D_\alpha(\mathbf{k}, \omega_m) = \det\underline{G}^{-1}(\mathbf{k}, \omega_m) = [i\omega_m Z_\alpha(\mathbf{k})]^2 - [\varepsilon_\alpha(\mathbf{k}) + X_\alpha(\mathbf{k}, \omega_m)]^2 - \Phi_\alpha(\mathbf{k}, \omega_m)^2 - \overline{\Phi_\alpha}(\mathbf{k}, \omega_m)^2$. Using Eqs. (A3) and (A5) we obtain the following self-consistent equations for the four unknown functions:

$$i\omega_m[1 - Z_\alpha(\mathbf{k})] = \frac{1}{\beta N_{k'}} \sum_{n,\beta,\mathbf{k}'} V_{\alpha\beta N}(\mathbf{k} - \mathbf{k}', \omega_m - \omega_n)$$
$$\times \frac{i\omega_n Z_\beta(\mathbf{k}')}{D_\beta(\mathbf{k}', \omega_n)},$$

$$X_\alpha(k, \omega_m) = \frac{1}{\beta N_{k'}} \sum_{n,\beta,\mathbf{k}'} V_{\alpha\beta N}(\mathbf{k} - \mathbf{k}', \omega_m - \omega_n)$$
$$\times \frac{\varepsilon_\beta(\mathbf{k}') + X_\beta(\mathbf{k}', \omega_n)}{D_\beta(\mathbf{k}', \omega_n)},$$

$$\Phi_\alpha(\mathbf{k}, \omega_m) = \frac{1}{\beta N_{k'}} \sum_{n,\beta,\mathbf{k}'} V_{\alpha\beta A}(\mathbf{k} - \mathbf{k}', \omega_m - \omega_n)$$
$$\times \frac{\Phi_\beta(\mathbf{k}', \omega_n)}{D_\beta(\mathbf{k}', \omega_n)},$$

$$\overline{\Phi_\alpha}(\mathbf{k}, \omega_m) = \frac{1}{\beta N_{k'}} \sum_{n,\beta,\mathbf{k}'} V_{\alpha\beta A}(\mathbf{k} - \mathbf{k}', \omega_m - \omega_n)$$
$$\times \frac{\overline{\Phi_\beta}(\mathbf{k}', \omega_n)}{D_\beta(\mathbf{k}', \omega_n)}. \quad (A7)$$

With the modified dispersion given by the poles of the Green's function, we define

$$E_\alpha(\mathbf{k}, \omega_n) = \sqrt{\frac{[\varepsilon_\alpha(\mathbf{k}) + X_\alpha(\mathbf{k}, \omega_n)]^2}{Z_\alpha(\mathbf{k})^2} + \frac{\Phi_\alpha(\mathbf{k}, \omega_n)^2 + \overline{\Phi_\alpha}(\mathbf{k}, \omega_n)^2}{Z_\alpha(\mathbf{k})^2}}. \quad (A8)$$

The normal state corresponds to a solution $\Phi = \overline{\Phi} = 0$. Z is the quasiparticle renormalization factor, and X describes shifts in the electron energies. The superconducting state is characterized by a nonzero Φ or $\overline{\Phi}$. From Eq. (A8) the gap function given by

$$\Delta_\alpha(\mathbf{k}, \omega_n) = \frac{\Phi_\alpha(\mathbf{k}, \omega_n) - i\overline{\Phi_\alpha}(\mathbf{k}, \omega_n)}{Z_\alpha(\mathbf{k})} \quad (A9)$$

describes the energy gap in the quasiparticle spectrum. $\Phi(\mathbf{k}, \omega_n)$ and $\overline{\Phi}(\mathbf{k}, \omega_n)$ obey the same equations and are expected to have the same functional form up to a common phase factor. This phase factor becomes important in the description of Josephson junctions, but is irrelevant for the thermodynamic properties of a homogeneous superconductor.

In the following we choose the simple gauge $\overline{\Phi}(\mathbf{k}, \omega_n) = 0$, rendering $\Delta_\alpha(\mathbf{k}, \omega_n) = \frac{\Phi_\alpha(\mathbf{k}, \omega_n)}{Z_\alpha(\mathbf{k})}$. We also rewrite $D_\alpha(\mathbf{k}, \omega_n) = [i\omega_n Z_\alpha(\mathbf{k})]^2 - [E_\alpha(\mathbf{k}, \omega_n)Z_\alpha(\mathbf{k})]^2$. For simplifying the self-consistent equations further, we will ignore $X_\alpha(\mathbf{k}, \omega_n)$ considering energy shifts to the dispersion being much smaller and negligible compared to the value of $\varepsilon_\alpha(\mathbf{k})$ itself. This leaves us with the following two equations to solve:

$$i\omega_m[1 - Z_\alpha(\mathbf{k})] = \frac{1}{\beta N_{k'}} \sum_{n,\beta,\mathbf{k}'} V_{\alpha\beta N}(\mathbf{k} - \mathbf{k}', \omega_m - \omega_n)$$
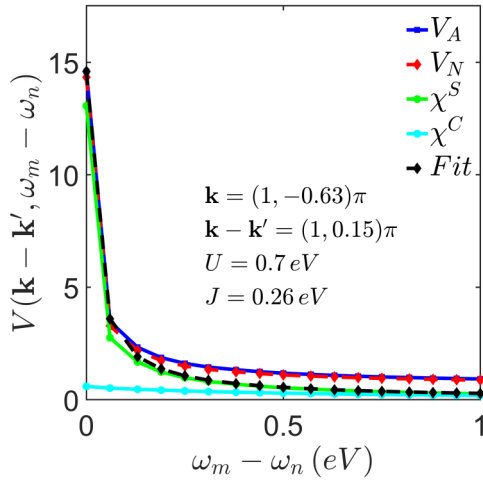$$\times \frac{i\omega_n}{Z_\beta(\mathbf{k}')[(i\omega_n)^2 - E_\beta(\mathbf{k}', \omega_n)^2]}, \quad (A10a)$$

FIG. 6. The frequency dependence of the effective interaction $V(\mathbf{k} - \mathbf{k}', \omega_m - \omega_n)$.

$$\Phi_\alpha(\mathbf{k}, \omega_m) = \frac{1}{\beta N_{k'}} \sum_{n, \beta, \mathbf{k}'} V_{\alpha\beta A}(\mathbf{k} - \mathbf{k}', \omega_m - \omega_n)$$

$$\times \frac{\Phi_\beta(\mathbf{k}', \omega_n)}{Z_\beta^2(\mathbf{k}')[(i\omega_n)^2 - E_\beta(\mathbf{k}', \omega_n)^2]}. \tag{A10b}$$

We will simplify the equations further, under assumptions at $T = T_C$, to obtain solutions without implementing numerically expensive self-consistency loops. The interaction vertices $V_{\alpha\beta N/A}(\mathbf{k} - \mathbf{k}', \omega_m - \omega_n)$ is expressed in terms of the spin fluctuation contribution $\chi_{\alpha\beta}^S(\mathbf{k} - \mathbf{k}', \omega_m - \omega_n)$ and the charge fluctuation contribution $\chi_{\alpha\beta}^C(\mathbf{k} - \mathbf{k}', \omega_m - \omega_n)$. Let us denote $(\omega_m - \omega_n)$ by Ω_{mn}. Figure 6 shows the Matsubara frequency dependence of these two terms and of the interaction vertices for a momentum transfer of $(\pi, 0.15\pi)$ (incommensurate antiferromagnetic wave vector) connecting the electron and hole pocket at a typical interaction strength for our multiorbital pnictide system. Here the spin fluctuation contribution is dominant and falls off on a frequency scale that is small compared with the bandwidth. Thus, the gap equation is dominated by important $\mathbf{k}$ and $\mathbf{k}'$ values restricted by this frequency cutoff to remain near Fermi surface. Without band crossing in the vicinity of the Fermi level, each FS point corresponds to a unique band quantum number, i.e., $\mathbf{k} \in \mu$, and $\mathbf{k}' \in \nu$. Henceforth, we transfer the band index as a subscript of momentum index $\mathbf{k}$.

For $\Omega_{mn} = 0$ in the Matsubara axis, the real quantity $V_{A/N}(\mathbf{k}_\mu - \mathbf{k}_\nu', \Omega_{mn} = 0)$ translates to the real part of the retarded quantity $\text{Re}[V_{A/N}(\mathbf{k}_\mu - \mathbf{k}_\nu', \Omega = 0)]$. We assume the form of the interaction to have the following explicit dependence on the Matsubara frequency:

$$V_{A/N}(\mathbf{k}_\mu - \mathbf{k}_\nu', \Omega_{mn}) = \frac{V_{A/N}(\mathbf{k}_\mu - \mathbf{k}_\nu', \Omega_{mn} = 0)}{1 + W|\Omega_{mn}|}$$

$$= \frac{\text{Re}[V_{A/N}(\mathbf{k}_\mu - \mathbf{k}_\nu', \Omega = 0)]}{1 + W|\omega_m - \omega_n|}, \tag{A11}$$

where $W \propto \xi_C^{-1}$, ξ_C being the spin-fluctuation energy cutoff. We show the band representation of the effective interaction vertices from orbital space in Eq. (7) in the main text. In Fig. 6 we also show the numerically fitted curve (in black) to the form of Eq. (A11). It shows good fit for low frequency region $|\omega_m - \omega_n| < \xi_C$ which makes the largest contribution to the frequency sum in Eqs. (A10a) and (A10b). As for the external frequency, we solve the Eliashberg equations for low energy physics at the Fermi level at $\omega_m = \omega_0 = \pi k_B T_C$ (lowest Fermionic Matsubara frequency). This makes $|\omega_m - \omega_n| = |\omega_0 - \omega_n| = |2n\pi k_B T_C|$. For simplicity, we assume that the gap function is frequency independent $\Phi_\mu(\mathbf{k}, \omega_n) = \Phi(\mathbf{k}_\mu)$.

First, we apply the above assumptions in d dimensions to Eq. (A10a):

$$\omega_0[1 - Z(\mathbf{k}_\mu)]$$

$$= -\frac{1}{\beta(2\pi)^d} \oint_{\mathbf{k}_\nu' \in FS} \frac{[V(\mathbf{k}_\mu, \mathbf{k}_\nu', 0)]_N}{|\mathbf{v}_F(\mathbf{k}_\nu')|} (d^{d-1}k_\nu')_\parallel$$

$$\times \sum_{n=-\infty}^{\infty} \frac{\omega_n}{1 + W|2n\pi k_B T_C|} \int_{-\infty}^{\infty} d\varepsilon_{k_\nu'}' \frac{1}{\omega_n^2 + \varepsilon_{k_\nu'}'^2}, \tag{A12}$$

$[V(\mathbf{k}_\mu, \mathbf{k}_\nu', 0)]_N$ is expressed in Eq. (7). The momentum summation over full BZ has been reduced to a transverse and longitudinal integration over the Fermi surface values of the quantities involved in the equation. At T_C, we have $\varepsilon(\mathbf{k}_\nu') \gg \Phi(\mathbf{k}_\nu')$, hence $E(\mathbf{k}_\nu', \omega_n) \approx \frac{\varepsilon(\mathbf{k}_\nu')}{Z(\mathbf{k}_\nu')} = \varepsilon_{k_\nu'}'$. Since the effective interaction is peaked mostly for scattering vectors connecting states $(\mathbf{k}_\mu, \mathbf{k}_\nu')$ on the FS, one can identify that the full BZ summation can be replaced by integration over small shells wrapped around the FS. Within the infinitesimal volume of each cubes surrounding individual FS points, we assume that there is only longitudinal variation of $[V(\mathbf{k}_\mu, \mathbf{k}_\nu', 0)]_N$, $Z(\mathbf{k}_\nu')$, and $\Phi(\mathbf{k}_\nu')$ parallel to the FS, and no variation in the transverse direction. Hence, they are constant within this infinitesimal cube at any FS point k_ν'. $\varepsilon_{k_\nu'}'$ is constant along the FS and only varies in the transverse direction. The integration yields $\frac{2}{|\omega_n|} \tan^{-1}(\infty) = \frac{\pi}{|\omega_n|}$ and together with the factor $1/\beta$ on the right-hand side it cancels the factor $\omega_0 = \pi k_B T_C = \pi/\beta$ on the left-hand side, while $\omega_n/|\omega_n|$ yields a $\text{sgn}(\omega_n)$ on the right-hand side. Equation (A12) is rewritten as

$$Z(\mathbf{k}_\mu) = 1 + \frac{1}{(2\pi)^d} \oint_{\mathbf{k}_\nu' \in FS} [V(\mathbf{k}_\mu, \mathbf{k}_\nu', 0)]_N \frac{(d^{d-1}k_\nu')_\parallel}{|\mathbf{v}_F(\mathbf{k}_\nu')|}$$

$$\times \sum_{n=-\infty}^{\infty} \frac{\text{sgn}(\omega_n)}{1 + W|2n\pi k_B T_C|}. \tag{A13}$$

The Matsubara sum just survives for $n = 0$ and is canceled out for all positive $(+n)$ and negative $(-n)$ pairs due to the oddness of $\text{sgn}(\omega_n)$. Thus, with $\text{sgn}(\omega_0) = +1$ we arrive at the following equation that needs to be numerically solved for $Z(\mathbf{k}_\mu)$:

$$Z(\mathbf{k}_\mu) = 1 + \frac{1}{(2\pi)^d} \oint_{\mathbf{k}_\nu' \in FS} [V(\mathbf{k}_\mu, \mathbf{k}_\nu', 0)]_N \frac{(d^{d-1}k_\nu')_\parallel}{|\mathbf{v}_F(\mathbf{k}_\nu')|}. \tag{A14}$$

Returning to Eq. (A10b), we proceed similarly as above:

$$\Phi(\mathbf{k}_\mu) = -\frac{\pi}{\beta(2\pi)^d} \oint_{\mathbf{k}'_\nu \in FS} \frac{[V(\mathbf{k}_\mu, \mathbf{k}'_\nu, 0)]_A \Phi(\mathbf{k}'_\nu)}{Z(\mathbf{k}'_\nu)} \frac{(d^{d-1}k'_\nu)_\parallel}{|\mathbf{v}_F(\mathbf{k}'_\nu)|} \sum_{n=-\infty}^{\infty} \frac{1}{1 + W|2n\pi k_B T_C|} \frac{1}{|\omega_n|}. \tag{A15}$$

We can perform the Matsubara sum. Rewriting in terms of the dimensionless parameter $A = 1/(2\pi W k_B T_C)$:

$$\frac{\pi}{\beta} \sum_{n=-\infty}^{\infty} \frac{1}{1 + |n|/A} \frac{1}{|\omega_n|} = \sum_{n=-\infty}^{\infty} \frac{A}{A + |n|} \frac{1}{|2n+1|} = \sum_{n=0}^{\infty} \frac{A}{A+1+n} \frac{1}{2n+1} + \sum_{n=0}^{\infty} \frac{A}{A+n} \frac{1}{2n+1}, \tag{A16}$$

where we shifted n to $(n-1)$ in the first infinite summation term. For low critical temperatures, $A \gg 1$, and we can absorb $A + 1 \approx A$ which gives

$$\frac{\pi}{\beta} \sum_{n=-\infty}^{\infty} \frac{1}{1 + |n|/A} \frac{1}{|\omega_n|} = 2 \sum_{n=0}^{\infty} \frac{A}{A+n} \frac{1}{2n+1}. \tag{A17}$$

We refer to identities of the Digamma function $\Psi(z)$, one of which is

$$\Psi(z) = -\gamma + \sum_{n=0}^{\infty} \frac{z-1}{(2n+1)(z+n)}, \tag{A18}$$

γ is the Euler-Macheroni constant. For $z \gg 1$, we have $z - 1 \approx z$ and $\Psi(z) \approx \log(z)$. Thus, rewriting Eq. (A17):

$$\frac{\pi}{\beta} \sum_{n=-\infty}^{\infty} \frac{1}{1 + |n|/A} \frac{1}{|\omega_n|} \approx 2[\gamma + \log(A)] = 2\log(e^\gamma A). \tag{A19}$$

This makes the linearized gap equation from Eq. (A15) take the following form:

$$\Phi(\mathbf{k}_\mu) = -\frac{2\log(e^\gamma A)}{(2\pi)^d} \oint_{\mathbf{k}'_\nu \in FS} \frac{[V(\mathbf{k}_\mu, \mathbf{k}'_\nu, 0)]_A}{Z(\mathbf{k}'_\nu)} \frac{(d^{d-1}k'_\nu)_\parallel}{|\mathbf{v}_F(\mathbf{k}'_\nu)|} \Phi(\mathbf{k}'_\nu). \tag{A20}$$

The gap equation above turns out to be an eigenvalue equation which can now be solved numerically, yielding eigenvalue λ and vector $g(\mathbf{k})$. Multiplying with $\oint_{\mathbf{k}_\mu \in FS} \frac{\Phi(\mathbf{k}_\mu)(d^{d-1}k_\mu)_\parallel}{(2\pi)^d |\mathbf{v}_F(\mathbf{k}_\mu)|}$ on both sides of the above equation, we get

$$\oint_{\mathbf{k}_\mu \in FS} \frac{(d^{d-1}k_\mu)_\parallel}{(2\pi)^d |\mathbf{v}_F(\mathbf{k}_\mu)|} \Phi^2(\mathbf{k}_\mu) = -\frac{2\log(e^\gamma A)}{(2\pi)^{2d}} \oint_{\mathbf{k}'_\nu \in FS} \oint_{\mathbf{k}_\mu \in FS} \frac{(d^{d-1}k_\mu)_\parallel}{|\mathbf{v}_F(\mathbf{k}_\mu)|} \Phi(\mathbf{k}_\mu) \frac{[V(\mathbf{k}_\mu, \mathbf{k}'_\nu, 0)]_A}{Z(\mathbf{k}'_\nu)} \frac{(d^{d-1}k'_\nu)_\parallel}{|\mathbf{v}_F(\mathbf{k}'_\nu)|} \Phi(\mathbf{k}'_\nu). \tag{A21}$$

Defining λ as

$$\lambda = -\frac{\frac{1}{(2\pi)^{2d}} \oint_{\mathbf{k}'_\nu \in FS} \oint_{\mathbf{k}_\mu \in FS} \frac{(d^{d-1}k_\mu)_\parallel}{|\mathbf{v}_F(\mathbf{k}_\mu)|} \Phi(\mathbf{k}_\mu) \frac{[V(\mathbf{k}_\mu, \mathbf{k}'_\nu, 0)]_A}{Z(\mathbf{k}'_\nu)} \frac{(d^{d-1}k'_\nu)_\parallel}{|\mathbf{v}_F(\mathbf{k}'_\nu)|} \Phi(\mathbf{k}'_\nu)}{\oint_{\mathbf{k}_\mu \in FS} \frac{(d^{d-1}k_\mu)_\parallel}{(2\pi)^d |\mathbf{v}_F(\mathbf{k}_\mu)|} \Phi^2(\mathbf{k}_\mu)}, \tag{A22}$$

and dropping the constant log term from our numerical solution, we get the following eigenvalue equation from Eq. (A20) that needs to be numerically evaluated:

$$\lambda g(\mathbf{k}_\mu) = -\frac{1}{(2\pi)^d} \sum_{\mathbf{k}'_\nu \in FS} \frac{1}{Z(\mathbf{k}'_\nu)} [V(\mathbf{k}_\mu, \mathbf{k}'_\nu, 0)]_A \frac{(d^{d-1}k'_\nu)_\parallel}{|\mathbf{v}_F(\mathbf{k}'_\nu)|} g(\mathbf{k}'_\nu). \tag{A23}$$

The final modified gap structure due to $Z(\mathbf{k}_\mu)$ is given by $\Delta(\mathbf{k}_\mu) = \frac{g(\mathbf{k}_\mu)}{Z(\mathbf{k}_\mu)}$.

---

[1] L. de Medici, *Iron-Based Superconductivity, Weak and Strong Correlations in Fe Superconductors*, edited by P. D. Johnson, G. Xu, and W.-G. Yin, Springer Series in Materials Science (Springer, Berlin, 2015).

[2] E. Bascones, B. Valenzuela, and M. J. Calderón, C. R. Phys. **17**, 36 (2016).

[3] A. van Roekeghem, P. Richard, H. Ding, and S. Biermann, C. R. Phys. **17**, 140 (2016).

[4] Z. P. Yin, K. Haule, and G. Kotliar, Nat. Mater. **10**, 932 (2011).

[5] Y. Li, Z. Yin, X. Wang, D. W. Tam, D. L. Abernathy, A. Podlesnyak, C. Zhang, M. Wang, L. Xing, C. Jin, K. Haule, G. Kotliar, T. A. Maier, and P. Dai, Phys. Rev. Lett. **116**, 247001 (2016).

[6] Z. R. Ye, Y. Zhang, F. Chen, M. Xu, J. Jiang, X. H. Niu, C. H. P. Wen, L. Y. Xing, X. C. Wang, C. Q. Jin, B. P. Xie, and D. L. Feng, Phys. Rev. X **4**, 031041 (2014).

[7] N. Arakawa and M. Ogata, J. Phys. Soc. Jpn. **80**, 074704 (2011).

[8] R. Yu, J.-X. Zhu, and Q. Si, Phys. Rev. B **89**, 024509 (2014).

[9] Z. P. Yin, K. Haule, and G. Kotliar, Nat. Phys. **10**, 845 (2014).

[10] P. O. Sprau, A. Kostin, A. Kreisel, A. E. Böhmer, V. Taufour, P. C. Canfield, S. Mukherjee, P. J. Hirschfeld, B. M. Andersen, and J. C. S. Davis, Science **357**, 75 (2017).

[11] D. J. Scalapino, Rev. Mod. Phys. **84**, 1383 (2012).

[12] P. J. Hirschfeld, C. R. Phys. **17**, 197 (2016).

[13] A. Chubukov, in *Iron-Based Superconductivity, Itinerant Electron Scenario for Fe-based Superconductors*, edited by P. D. Johnson, G. Xu, and W.-G. Yin, Springer Series in Materials Science (Springer, Berlin, 2015).

[14] I. I. Mazin, D. J. Singh, M. D. Johannes, and M. H. Du, Phys. Rev. Lett. **101**, 057003 (2008).

[15] T. A. Maier, S. Graser, D. J. Scalapino, and P. J. Hirschfeld, Phys. Rev. B **79**, 224510 (2009).

[16] A. Kreisel, B. M. Andersen, P. O. Sprau, A. Kostin, J. C. S. Davis, and P. J. Hirschfeld, Phys. Rev. B **95**, 174504 (2017).

[17] G. Lee, H. S. Ji, Y. Kim, C. Kim, K. Haule, G. Kotliar, B. Lee, S. Khim, K. H. Kim, K. S. Kim, K.-S. Kim, and J. H. Shim, Phys. Rev. Lett. **109**, 177001 (2012).

[18] J. Ferber, K. Foyevtsova, R. Valentí, and H. O. Jeschke, Phys. Rev. B **85**, 094505 (2012).

[19] S. V. Borisenko, V. B. Zabolotnyy, D. V. Evtushinsky, T. K. Kim, I. V. Morozov, A. N. Yaresko, A. A. Kordyuk, G. Behr, A. Vasiliev, R. Follath, and B. Büchner, Phys. Rev. Lett. **105**, 067002 (2010).

[20] S. V. Borisenko, V. B. Zabolotnyy, A. A. Kordyuk, D. V. Evtushinsky, T. K. Kim, I. V. Morozov, R. Follath, and B. Büchner, Symmetry **4**, 251 (2012).

[21] K. Zantout, S. Backes, and R. Valentí, Phys. Rev. Lett. **123**, 256401 (2019).

[22] C. Platt, R. Thomale, and W. Hanke, Phys. Rev. B **84**, 235121 (2011).

[23] Y. Wang, A. Kreisel, V. B. Zabolotnyy, S. V. Borisenko, B. Büchner, T. A. Maier, P. J. Hirschfeld, and D. J. Scalapino, Phys. Rev. B **88**, 174516 (2013).

[24] T. Saito, S. Onari, Y. Yamakawa, H. Kontani, S. V. Borisenko, and V. B. Zabolotnyy, Phys. Rev. B **90**, 035104 (2014).

[25] F. Ahn, I. Eremin, J. Knolle, V. B. Zabolotnyy, S. V. Borisenko, B. Büchner, and A. V. Chubukov, Phys. Rev. B **89**, 144513 (2014).

[26] M. P. Allan, A. W. Rost, A. P. Mackenzie, Y. Xie, J. C. Davis, K. Kihou, C. H. Lee, A. Iyo, H. Eisaki, and T.-M. Chuang, Science **336**, 563 (2012).

[27] K. Umezawa, Y. Li, H. Miao, K. Nakayama, Z.-H. Liu, P. Richard, T. Sato, J. B. He, D.-M. Wang, G. F. Chen, H. Ding, T. Takahashi, and S.-C. Wang, Phys. Rev. Lett. **108**, 037002 (2012).

[28] H. Ikeda, J. Phys. Soc. Jpn. **77**, 123707 (2008).

[29] H. Ikeda, R. Arita, and J. Kuneš, Phys. Rev. B **81**, 054502 (2010).

[30] Y. Yanagi, Y. Yamakawa, N. Adachi, and Y. Ōno, Phys. Rev. B **82**, 064518 (2010).

[31] K. Kuroki, S. Onari, R. Arita, H. Usui, Y. Tanaka, H. Kontani, and H. Aoki, Phys. Rev. Lett. **101**, 087004 (2008).

[32] C. Triola, J. Cayao, and A. M. Black-Schaffer, Ann. Phys. **532**, 1900298 (2020).

[33] S. Maiti, M. M. Korshunov, T. A. Maier, P. J. Hirschfeld, and A. V. Chubukov, Phys. Rev. Lett. **107**, 147002 (2011).